DR CRAIG J GALBAN (Orcid ID : 0000-0001-5596-7487)

Article type : O - Original Article

Multicenter Evaluation of Parametric Response Mapping as an Indicator of Bronchiolitis Obliterans Syndrome After Hematopoietic Stem Cell Transplantation

Guang-Shing Cheng[1], Katherine E. Selwa[2], Charles Hatt[3], Sundaresh Ram[4], Aleksa B. Fortuna[4], Margaret Guerriero[5], Ben Himelhoch[6], Daniel McAree[7], Timothy C Hoffman[2], Joseph Brisson[8], Ryan Nazareno[8], Kiernan Bloye[8], Timothy D. Johnson[9], Mats Remberger[10], Jonas Mattsson[10], Dharshan Vummidi[4], Ella E. Kazerooni[4], Vibha N. Lama[11], Stefanie Galban[4], Michael Boeckh[1], Gregory A. Yanik[8], Craig J. Galban[4]

[1]Clinical Research Division, Fred Hutchinson Cancer Research Center, Seattle, Washington
[2]University of Michigan Medical School, Ann Arbor, Michigan
[3]Imbio, LLC Minneapolis, Minnesota
[4]Department of Radiology, Michigan Medicine, Ann Arbor, Michigan
[5]Seattle Cancer Care Alliance, Seattle, Washington
[6]Michigan State University College of Human Medicine, Lansing, Michigan
[7]Pediatrics, University of Michigan, Ann Arbor, Michigan
[8]Blood and Marrow Transplant Program, Michigan Medicine, Ann Arbor, Michigan
[9]Department of Biostatistics, University of Michigan School of Public Health, Ann Arbor, Michigan
[10]Department of Oncology-Pathology, Karolinska University Hospital, Stockholm, Sweden
[11]Division of Pulmonary and Critical Care Medicine, Michigan Medicine, Ann Arbor, Michigan

Gregory A. Yanik and Craig J. Galban share senior authorship.

Correspondence

Craig J. Galban
Email: cgalban@med.umich.edu

Abbreviations:

BOS Bronchiolitis Obliterans Syndrome
COPD Chronic Obstructive Pulmonary Disease
CT Computed Tomography
Emph Emphysematous Lung Parenchyma
FEV1 Forced Expiratory Volume at 1 second
FH Fred Hutchinson Cancer Research Center
FRC Functional Residual Capacity
fSAD Functional Small Airways Disease
FVC Forced Vital Capacity
HCT Hematopoietic Stem Cell Transplantation
HU Hounsfield Unit
KI Karolinska University Hospital
Norm Normal Lung Parenchyma
PD Parenchymal Disease
PRM Parametric Response Mapping
SAD Small airways disease
TLC Total Lung Capacity
UM University of Michigan
VOI Volume of Interest

ABSTRACT

Parametric response mapping (PRM) is a novel computed tomography (CT) technology which has shown potential for assessment of bronchiolitis obliterans syndrome (BOS) after hematopoietic stem cell transplantation (HCT). The primary aim of the current study was to evaluate if variations in image acquisition under real world conditions affect the PRM measurements of clinically diagnosed BOS. CT scans were obtained retrospectively from 72 HCT recipients with BOS and graft-versus-host disease from Fred Hutchinson Cancer Research Center, Karolinska Institute and the University of Michigan. Whole lung volumetric scans were performed at inspiration and expiration using site-specific acquisition and reconstruction protocols. PRM and pulmonary function measurements were assessed. Patients with

moderately severe BOS at diagnosis (median FEV1 53.5% predicted) had similar characteristics between sites. Variations in site-specific CT acquisition protocols had a negligible effect on the PRM-derived small airways disease (SAD), i.e. BOS, measurements. PRM-derived SAD was found to correlate with FEV1 % predicted and FEV1/FVC (R=-0.236, p=0.046; and R=-0.689, p<0.0001, respectively), which suggests that elevated levels in the PRM measurements is primarily affected by BOS airflow obstruction and not CT scan acquisition parameters. Based on these results, PRM may be applied broadly for post-HCT diagnosis and monitoring of BOS.

INTRODUCTION

Bronchiolitis obliterans syndrome (BOS) is a chronic obstructive airway disease associated with chronic graft-versus-host disease (GVHD) that occurs in 5-12% of allogeneic hematopoietic cell transplant (allo-HCT) recipients [1-7]. The disorder is characterized by progressive fibro-obliteration of terminal bronchioles, with resultant air trapping, progressive dyspnea, recurrent pulmonary infections and an overall decrease in quality of life as well as increased nonrelapse mortality [8]. Most patients do not come to clinical attention until symptoms arise, at which point lung function decline is already severe and irreversible. The ability to identify and treat patients earlier in their clinical course is critical to reducing the morbidity and mortality associated with this condition [9]. The NIH consensus guidelines for the diagnosis of chronic GVHD, however, do not allow for recognition of early BOS, atypical phenotypes of airflow obstruction, or restrictive lung disease (RLD)[10]. Novel imaging biomarkers that can serve as an adjunct to standard spirometry are needed to improve the assessment of early disease.

Parametric Response Mapping (PRM) is a voxel-based approach for analyzing high resolution x-ray computed tomography (HRCT) images that provides detailed information on disease phenotype otherwise unattainable by conventional CT-based quantitative measures [11]. Using inspiratory and expiratory HRCT scans, PRM allows for the quantification of small airway disease (SAD) that contributes to airflow obstruction. PRM has been developed as a quantitative imaging biomarker for the assessment of obstructive lung disease in both chronic obstructive pulmonary disease (COPD) [11] and BOS post-lung allografts [12, 13]. The potential utility of PRM for assessing SAD due to BOS after HCT has been recently examined in a single center cohort of BOS after allo-HCT with and without the presence of infection. Although a specific PRM signature was capable of identifying BOS even in the presence of interstitial pneumonitis in HCT recipients from a single site [14], variability in CT acquisition may affect the ability to apply PRM CT scans acquired at multiple sites. The primary aim of the current study was to evaluate if variations in image acquisition under real world conditions affect the PRM measurements of

clinically diagnosed BOS. In addition, we describe features of PRM that may distinguish between phenotypes of BOS and RLD potentially related to chronic GVHD.

MATERIALS AND METHODS

Subjects

Allo-HCT recipients diagnosed with BOS were accrued as part of a multi-center retrospective observational study. Participating sites included the Karolinska University Hospital (KI), Fred Hutchinson Cancer Research Center (FH), and University of Michigan (UM). Any patient with a clinical diagnosis of BOS between the years of 2000 and 2015, with a high-resolution chest CT and a pulmonary function test within 28 days of BOS diagnosis, were included. Additional subjects with chronic GVHD and restrictive lung disease were also included for an exploratory analysis. The study was approved by the Institutional Review Boards at all participating sites. In addition, all patients had signed an IRB-approved informed consent for data collection and analysis.

PFTs were obtained as per clinical care guidelines of each respective institution. Forced expiratory volume in 1 second percent predicted (FEV1%), forced vital capacity percent predicted (FVC%), FEV1/FVC ratio and total lung capacity (TLC) were based on accepted reference values that reflected the population served by each institution (**Table 1**). The clinical diagnosis of BOS was established on a site-by-site basis through clinical care. These criteria included modified NIH consensus criteria: FEV1 < 75% predicted, signs of obstructive airway disease (FEV1/FVC ratio <.7, residual volume >120% predicted, or evidence of air trapping on high-resolution CT), absence of infection, and the presence of chronic graft-versus-host disease in another organ [15]. Additional criteria for BOS diagnosis included decline in FEV1 and FVC with normal TLC, in the absence of infection or other causes for airflow decline[16], as well as those with mixed obstructive and restrictive ventilatory impairment based on obstruction by FEV1/FVC ratio <0.7 or elevated RV with a concomitant decline in TLC. A small subset of patients with restrictive physiology in the presence of chronic GVHD were also included (N=3 RLD only and N=8 BOS/RLD).

CT Acquisition

CT examinations were performed using site-specific acquisition and reconstruction protocols (**Supplemental Table 1**). For all sites, paired CT scans were acquired at full inspiration (total lung capacity, TLC) and relaxed expiration (functional residual capacity, FRC). Quantitative CT data were presented in Hounsfield units (HU), where stability of CT

measurement for each scanner was monitored based on site-specific protocols. For reference, air, water and blood attenuation values should be -1000, 0 and 50 HU, respectively [17].

Parametric Response Mapping

PRM was applied to all paired CT scans as previously described [11, 14]. Briefly, lungs from both paired CT scans were segmented from the thoracic cavity using an in-house algorithm written in Matlab (The MathWorks, Inc., Natick, MA). The whole-lung inspiratory CT scan was spatially aligned to the expiratory CT scan using Elastix, an open source image registration algorithm [18, 19]. This process allows the paired images to share the same geometric space, where each voxel, the smallest unit of volume in a three-dimensional image dataset, consists of HU values at inspiration and expiration. To mitigate the effects of noise on the PRM analysis, a 3x3 median filter was applied to all slices in the paired CT scans. Finally, all voxels bounded between -1000 and -250 HU on both paired CT scans were classified based on a scheme of three predetermined thresholds as previously described [14]. Voxels with values greater than or equal to -950 HU and less than -810 HU at inspiration and greater than or equal to -856 HU at expiration were classified normal (PRM^{Norm}, green voxels), greater than or equal to -950 HU and less than -810 HU at inspiration and less than -856 HU at expiration were functional small airways disease (PRM^{fSAD}, yellow voxels), less than -950 HU at inspiration and less than -856 HU at expiration were emphysema (PRM^{Emph}, red voxels), and greater than or equal to -810 HU at inspiration were parenchymal disease (PD) (PRM^{PD}, purple voxels). The relative lung volumes, calculated as the sum of all voxels within a class normalized to the sum of all voxels within the expiratory lungs multiplied by 100, were used as global measures.

Statistical Analysis

All data values are presented as the mean ± standard deviation, unless specified otherwise. Site comparisons were determined for all variables, i.e. mean and standard deviation of HU values, patient characteristics, and PFT and PRM measures. Analysis of variance, controlling for multiple comparisons using a Bonferroni post-hoc test, and χ^2 tests were used to assess site differences in continuous and categorical variables, respectively. Paired student's t-test was used to assess differences in the mean HU of ambient and tracheal air measured on inspiration and expiration CT scans from each site. PRM measures were correlated to PFT outcomes using a non-parametric Spearman rho correlation. Finally, multivariable analyses were performed using an ANCOVA to determine the contribution of PRM^{fSAD} and PRM^{PD}, controlling for site and BMI, to FEV1%, FVC%, FEV1/FVC and TLC. Results were considered statistically significant at the 2-sided 5% comparison-wise significance level ($P < .05$). All statistical computations were performed with a statistical software package (IBM SPSS

Statistics, v. 21, Armonk, NY). Box and whiskers plots, generated using GraphPad Prism 7 (San Diego, CA), are presented as the 25th and 75th percentiles for the lower and upper box, respectively, median value for the line in the box, 5th and 95th percentiles for lower and upper whiskers, respectively, and markers as outliers.

RESULTS

Subject and Site Characteristics

Seventy-two patients were enrolled, including 12 patients from KI, 48 patients from FH, and 12 patients from UM (**Table 1**). The KI cohort included 6 subjects with BOS, including 3 with mixed obstruction/restriction and 3 patients with GVHD who had restriction on PFT. The FH cohort were all clinically identified as BOS with airflow obstruction, including 5 patients with mixed obstruction/restriction. The UM cohort were identified as BOS and all had obstruction. Negligible differences were observed between patient characteristics. FH patients were diagnosed up to 1.08 and 1.71 (p=0.04) years later than patients diagnosed at KI and UM, respectively. The median FEV1% predicted at diagnosis were 49.5% (IQR = 21.8%), 54.9% (IQR = 25.8%) and 61.0% (IQR = 22.5%) for KI, FH and UM, respectively. In addition, there were no site differences in TLC. Significantly higher median FVC% and lower median FEV1/FVC were observed in the FH cohort (81.5%, IQR 23.5% and 0.55, IQR 0.25, respectively) when compared to KI (65.5%, IQR 23.0% and 0.72, IQR 0.29, respectively). Significant variations in the acquisition and reconstruction of chest CT scans between and within sites were observed. Representative CT slices acquired at full inspiration and expiration demonstrate the effect of imaging protocol on image quality and noise (**Figure 1A and B)**. Details regarding the technical aspects of the CT reconstructions and analyses are provided in the **Supplemental** section.

Presented in **Figure 1C and D** are examples of PRM images with corresponding scatter plots of individual lung voxels. All subjects had elevated levels of fSAD (the relative volume of lung with voxels greater than or equal to -950 HU and less than -810 HU at inspiration and less than -856 at expiration) than what is observed from a healthy population [PRM-derived fSAD = 5-15%, [12-14]]. On close examination of **Figure 1C**, PRM data for the KI case showed less spatial consolidation (i.e. noisier) of individual classifications as compared to the representative cases at FH and UM. **Figure 2** shows the relative volume of PRM-derived Normal, fSAD and PD for all subjects separated by site. Although the relative volumes of normal and diseased parenchyma were found to differ between sites, these results were not significant. FH was found to have higher, yet non-significant, values in fSAD compared to KI and UM. PRM-derived fSAD

and PD from all three sites were found to be elevated compared to healthy smokers (8.4±1% for fSAD and 11±2% for PD) reported in our previous work [14]. PRM-derived emphysema measurements (data not shown) were found to be significantly different between KI (4.0%±5.3%) and FH (0.9%±1.4%l p=0.001) and UM (1.4%±1.7%; p=0.04). Although the differences were significant, these values were small relative to PRM-derived fSAD and PD. All CT scans were radiographically confirmed by a trained thoracic radiologist (DV) to be absent of emphysema, which suggests that site differences in the relative volume of emphysema are most likely attributed to the higher HU scatter observed in the KI scans (**Figure 1** and **Supplemental Figure 1**).

Effect of Disease Severity and Phenotype on PRM

Analyses were performed to identify the contribution of disease severity and phenotype, as defined by PFT, on PRM measurements. **Figure 3** illustrates the relationship between PRM-derived fSAD and PD over the entire study cohort. As expected, most cases had high levels of fSAD (i.e. obstructive phenotype). Nevertheless, there were 18 cases, primarily from KI and FH, that were found to have PD levels > 20% with relatively low levels of fSAD (<20%), which included six cases of mixed (N=3) and restrictive (N=3) physiology by PFT.

The ability of PRM to differentiate the restrictive and obstructive phenotypes was further evaluated by comparing PRM-derived fSAD (obstructive component) and PD (restrictive component) to PFT measurements pooled over all three sites (**Table 2**). As expected, a drop in FEV1% was found to correspond with an increase in PRM-derived fSAD (R=-0.236, p=0.046). Likewise, for FEV1/FVC, a negative correlation was observed for fSAD (R=0.-689, p<0.0001) (**Supplemental Figure 2**), whereas a positive correlation was observed for PD (R=0.437, p<0.0001). These trends reversed when comparing PRM metrics to FVC% (fSAD: R=0.407, p,0.0001; PD: R=-0.486, p<0.0001 and TLC (fSAD: R=0.623, p<0.0001; PD: R=-0.531, p<0.0001). Performing the same analysis over individual site populations found similar correlations between PRM metrics and PFT measurement for KI and FH . UM correlations were only observed between fSAD and both FEV1% and FEV1/FVC; of note all the UM subjects had obstruction.

To determine the contribution of PRM-derived fSAD and PD on these PFT metrics, a multivariable analysis was performed controlling for site and BMI (**Table 3**). Although in a univariate analysis only fSAD was found to correlate with FEV1% (data not shown), both fSAD and PD were found to be strong parameters for FEV1%. Similar to the univariate analysis, PD and fSAD were strong contributors to statistical models of FVC% and FEV1/FVC, respectively.

This is consistent with the negative correlation observed in the univariate analysis. TLC was only found to correlate with PRM-derived fSAD.

DISCUSSION

In this retrospective analysis, we found that high resolution chest CT images of patients clinically diagnosed primarily with BOS from 3 centers could be analyzed by PRM for a small airways disease signature. Variations in the acquisition of CT images across centers accounted for variation in the image quality. Acquisition with reduced tube current and variations in expiration appeared to affect image quality and likely accounted for background ambient noise (**Supplemental** Section). Nevertheless, these variations did not diminish the overall ability of PRM to distinguish small airways disease from normal and parenchymal disease. Additionally, PRM suggested a signature for restrictive physiology, as the FVC and TLC negatively correlated with a parenchymal signature. RLD likely represents a manifestation of chronic GVHD in HCT recipients, analogous to "restrictive allograft syndrome" phenotype of chronic lung allograft dysfunction described in lung transplant recipients[20]. In a prospective European cohort, interstitial lung disease represented 21% of the late-onset noninfectious lung complications after allogeneic HCT, and were associated with a prior diagnosis of chronic GVHD[7]. Defining the mixed and restrictive PRM phenotypes of lung disease related to chronic GVHD will require additional work with a larger cohort.

Parametric response mapping of paired CT has been investigated extensively as an analytical technique to better phenotype airway obstruction in COPD [21-26]. Most of these studies are associated with multi-center observational trials such as the COPDGene and SPIROMICS [27, 28], where imaging protocols are selected to produce image quality consisted across participating sites. This allows consistent results in quantitative CT measures (e.g. PRM) across participating centers. The impact of image protocol variability on PRM measurements has been previously evaluated, but only in the context of COPDGene and SPIROMICS CT acquisitions [29]. Imaging protocols associated with large multi-center clinical trials do not necessarily reflect local practices of individual hospitals. Nevertheless, our single center studies have demonstrated PRM as a diagnostic imaging signature in BOS after HCT and lung transplant [12-14], which has the potential to aide in the evaluation and the definition of BOS. Given the potential variability of CT imaging protocols at different transplant centers, it was important to investigate the impact of technical and clinical factors on the PRM analysis.

Baseline chest CT image quality was found to vary from site to site and were most pronounced within the expiratory scans. Although acquisition and reconstruction parameters

varied between sites (**Supplemental Table 1**), this did not appear to affect whole-lung PRM values of fSAD and PD. In fact, results presented in this study suggest that variations in PRM-derived fSAD and PD are driven more by disease severity and phenotype, as shown by the differences in the PFT parameters of participants at each site. Conventional indices of airways obstruction, including FEV1 and FEV1/FVC, remain independently associated with fSAD signatures when site and BMI are taken into account. Correlations of these measures with pulmonary function measurements have shown PRM-derived fSAD and PD to obstructive and restrictive diseases. The observed correlations of fSAD and PD with pulmonary function parameters are consistent with a previously reported study evaluating PRM as a diagnostic biomarker of obstructive and restrictive lung disease in lung transplant recipients with GVHD [13]. Multivariable analysis of PRM measures, controlling for site of accrual, found that PRM-derived fSAD and PD are independent measures of disease severity and phenotype (**Table 2**).

The current study has several limitations. First, this is a retrospective study and CT scans were not originally acquired for the purposes of PRM case-control analysis. Due to the wide variability in scanner type, acquisition and reconstruction, there was insufficient number of cases to fully evaluate each of the many parameters that effect PRM measurements. This also made in infeasible to acquire controls, i.e. HCT recipients without GVHD scanned using a similar CT protocol, from the three centers that participated in this study. The cohort analysis was skewed to FH, which had significantly more patients than the other sites. It is possible that the difference in demographics were responsible for the variations in the PRM signatures. The number of cases was limited for an exploration of restrictive phenotypes. Nonetheless, the purpose of the study was to establish PRM as a valid technique for the diagnosis of clinically recognized BOS, and the study reflects real world conditions in which heterogeneous phenotypes of BOS exist [16] and different centers will serve populations reflective of that region. The correlation between PRM and PFT measures and PRM-derived fSAD and PD, regardless of site, suggests that PRM will still be diagnostically useful in multiple settings.

For PRM to be broadly applicable and diagnostically accurate, particularly for the diagnosis of early stage disease, it may be helpful to clarify the protocol requirements for a high-resolution CT imaging and to standardize the acquisition of high-resolution CT images. Based on the results reported in this study, sufficiently high x-ray tube currents, even if incremental scans are required to reduce x-ray exposure, is recommended for minimizing image noise which would improve PRM measurements. Although recent studies evaluating the utility of PRM as an early detector of BOS is promising, prospective studies in which HRCT are using for screening

of patients at risk for pulmonary graft-versus-host disease will help validate the use of PRM for early detection of disease onset and progression.

ACKNOWLEDGMENTS

This work was supported by the US National Institutes of Health research grants R44HL118837, R44HL140894, R01HL139690, R35CA197701, P30CA015704, and P30CA046592.

DISCLOSURE

The authors of this manuscript have conflicts of interest to disclose as described by the *American Journal of Transplantation.* CJG have a financial interest in Imbio, LLC, which has licensed the PRM technology. The other authors have no conflicts of interest to disclose.

FIGURE LEGENDS

Figure 1: Effect of site-specific imaging protocol on PRM. Presented are representative axial slices from CT scans acquired at (**A**) inspiration, (**B**) expiration, (**C**) PRM overlay and (**D**) corresponding PRM scatter plot. from an individual case at each participating site. Peak voltage, tube current, slice thickness and slice number/arrangement varied between cases. For the inspiration CT scan protocol parameters were: (KI) 120 kVp, 249 mA, 0.6 mm, 708/contiguous; (FH) 120 kVp, 410 mA, 1.25 mm, 122/contiguous; and (UM) 120 kVp, 372 mA, 1.25 mm, 521/contiguous. For the expiration CT scan protocol parameters were: (KI) 120 kVp, 66 mA, 0.6 mm, 635/contiguous; (FH) 120 kVp, 180 mA, 1.25 mm, 12/incremental; and (UM) 120 kVp, 376 mA, 1.25 mm, 502/contiguous. PRM-derived values over the whole lung are provided within an insert above each PRM image. The green value and markers represent normal parenchyma, yellow value and markers represent fSAD (i.e. BOS) and magenta value and markers represent parenchymal disease. Age, gender and percent predicted values of FEV1 and FVC for each case were: (KI) 63 yrs, male, 40% and 62%; (FH) 57 yrs, male, 71% and 94%; and (UM) 68 yrs, male, 44% and 71%.

Figure 2: Evaluation of the site differences in PRM measurements. Box and whisker plots are presented for the relative volume of PRM-derived measurements from paired CT scans acquired at each site. The line within the box, the box extremes and whiskers represent the median value, 25%ile and 75%ile, and 5%ile and 95%ile, respectively. Markers represent

outlies beyond 5%ile and 95%ile. Site differences in variables were tested using a univariable ANOVA controlling for multiple comparisons using the Bonferonni posthoc test. Significance was assessed at a p-value of 0.05. No significant differences were observed between sites for the presented measurements.

Figure 3: Contributions of PRM-derived fSAD and PD in cohort. Presented is a plot of the relative volumes of fSAD (PRM^{fSAD}) and PD (PRM^{PD}) for each of the 72 subjects studied with color-coding for site accrual. A clear trend between the contribution of fSAD and PD is observed.

REFERENCES

1. Williams KM CJ, Gladwin MT, Pavletic SZ. Bronchiolitis obliterans after allogeneic hematopoietic stem cell transplantation. JAMA. 2009;302(3):306-14.

2. Au BK, Au MA, Chien JW. Bronchiolitis obliterans syndrome epidemiology after allogeneic hematopoietic cell transplantation. Biol Blood Marrow Transplant. 2011;17(7):1072-8. doi: 10.1016/j.bbmt.2010.11.018. PubMed PMID: 21126596; PMCID: 3061253.

3. Chien JW, Duncan S, Williams KM, Pavletic SZ. Bronchiolitis obliterans syndrome after allogeneic hematopoietic stem cell transplantation-an increasingly recognized manifestation of chronic graft-versus-host disease. Biol Blood Marrow Transplant. 2010;16(1 Suppl):S106-14. doi: 10.1016/j.bbmt.2009.11.002. PubMed PMID: 19896545; PMCID: 3189470.

4. Hildebrandt GC, Fazekas T, Lawitschka A, Bertz H, Greinix H, Halter J, Pavletic SZ, Holler E, Wolff D. Diagnosis and treatment of pulmonary chronic GVHD: report from the consensus conference on clinical practice in chronic GVHD. Bone Marrow Transplant. 2011. Epub 2011/03/29. doi: bmt201135 [pii]
10.1038/bmt.2011.35. PubMed PMID: 21441964.

5. Williams KM. How I treat bronchiolitis obliterans syndrome after hematopoietic stem cell transplantation. Blood. 2017;129(4):448-55. doi: 10.1182/blood-2016-08-693507. PubMed PMID: 27856461; PMCID: PMC5270387.

6. Yanik G, Kitko C. Management of noninfectious lung injury following hematopoietic cell transplantation. Curr Opin Oncol. 2013;25(2):187-94. doi: 10.1097/CCO.0b013e32835dc8a5. PubMed PMID: 23340330.

7. Bergeron A, Chevret S, Peffault de Latour R, Chagnon K, de Margerie-Mellon C, Riviere F, Robin M, Mani J, Lorillon G, Socie G, Tazi A. Noninfectious lung complications after

allogeneic haematopoietic stem cell transplantation. Eur Respir J. 2018;51(5). doi: 10.1183/13993003.02617-2017. PubMed PMID: 29650555.

8. Bergeron A, Cheng GS. Bronchiolitis Obliterans Syndrome and Other Late Pulmonary Complications After Allogeneic Hematopoietic Stem Cell Transplantation. Clin Chest Med. 2017;38(4):607-21. doi: 10.1016/j.ccm.2017.07.003. PubMed PMID: 29128013.

9. Cheng GS, Storer B, Chien JW, Jagasia M, Hubbard JJ, Burns L, Ho VT, Pidala J, Palmer J, Johnston L, Mayer S, Crothers K, Pusic I, Lee SJ, Williams KM. Lung Function Trajectory in Bronchiolitis Obliterans Syndrome after Allogeneic Hematopoietic Cell Transplant. Ann Am Thorac Soc. 2016;13(11):1932-9. doi: 10.1513/AnnalsATS.201604-262OC. PubMed PMID: 27513368; PMCID: PMC5122479.

10. Jagasia MH, Greinix HT, Arora M, Williams KM, Wolff D, Cowen EW, Palmer J, Weisdorf D, Treister NS, Cheng GS, Kerr H, Stratton P, Duarte RF, McDonald GB, Inamoto Y, Vigorito A, Arai S, Datiles MB, Jacobsohn D, Heller T, Kitko CL, Mitchell SA, Martin PJ, Shulman H, Wu RS, Cutler CS, Vogelsang GB, Lee SJ, Pavletic SZ, Flowers ME. National Institutes of Health Consensus Development Project on Criteria for Clinical Trials in Chronic Graft-versus-Host Disease: I. The 2014 Diagnosis and Staging Working Group Report. Biol Blood Marrow Transplant. 2014. doi: 10.1016/j.bbmt.2014.12.001. PubMed PMID: 25529383.

11. Galban CJ, Han MK, Boes JL, Chughtai KA, Meyer CR, Johnson TD, Galban S, Rehemtulla A, Kazerooni EA, Martinez FJ, Ross BD. Computed tomography-based biomarker provides unique signature for diagnosis of COPD phenotypes and disease progression. Nat Med. 2012;18(11):1711-5. doi: 10.1038/nm.2971. PubMed PMID: 23042237; PMCID: PMC3493851.

12. Verleden SE, Vos R, Vandermeulen E, Ruttens D, Bellon H, Heigl T, Van Raemdonck DE, Verleden GM, Lama V, Ross BD, Galban CJ, Vanaudenaerde BM. Parametric Response Mapping of Bronchiolitis Obliterans Syndrome Progression After Lung Transplantation. Am J Transplant. 2016;16(11):3262-9. doi: 10.1111/ajt.13945. PubMed PMID: 27367568; PMCID: PMC5083149.

13. Belloli EA, Degtiar I, Wang X, Yanik GA, Stuckey LJ, Verleden SE, Kazerooni EA, Ross BD, Murray S, Galban CJ, Lama VN. Parametric Response Mapping as an Imaging Biomarker in Lung Transplant Recipients. Am J Respir Crit Care Med. 2017;195(7):942-52. Epub 2016/10/26. doi: 10.1164/rccm.201604-0732OC. PubMed PMID: 27779421; PMCID: PMC5387704.

14. Galban CJ, Boes JL, Bule M, Kitko CL, Couriel DR, Johnson TD, Lama V, Telenga ED, van den Berge M, Rehemtulla A, Kazerooni EA, Ponkowski MJ, Ross BD, Yanik GA. Parametric

response mapping as an indicator of bronchiolitis obliterans syndrome after hematopoietic stem cell transplantation. Biol Blood Marrow Transplant. 2014;20(10):1592-8. doi: 10.1016/j.bbmt.2014.06.014. PubMed PMID: 24954547; PMCID: PMC4163140.

15. Jagasia MH, Greinix HT, Arora M, Williams KM, Wolff D, Cowen EW, Palmer J, Weisdorf D, Treister NS, Cheng GS, Kerr H, Stratton P, Duarte RF, McDonald GB, Inamoto Y, Vigorito A, Arai S, Datiles MB, Jacobsohn D, Heller T, Kitko CL, Mitchell SA, Martin PJ, Shulman H, Wu RS, Cutler CS, Vogelsang GB, Lee SJ, Pavletic SZ, Flowers ME. National Institutes of Health Consensus Development Project on Criteria for Clinical Trials in Chronic Graft-versus-Host Disease: I. The 2014 Diagnosis and Staging Working Group Report. Biol Blood Marrow Transplant. 2015;21(3):389-401 e1. doi: 10.1016/j.bbmt.2014.12.001. PubMed PMID: 25529383; PMCID: 4329079.

16. Bergeron A, Godet C, Chevret S, Lorillon G, Peffault de Latour R, de Revel T, Robin M, Ribaud P, Socie G, Tazi A. Bronchiolitis obliterans syndrome after allogeneic hematopoietic SCT: phenotypes and prognosis. Bone Marrow Transplant. 2013;48(6):819-24. doi: 10.1038/bmt.2012.241. PubMed PMID: 23208317.

17. Stoel BC, Stolk J. Optimization and standardization of lung densitometry in the assessment of pulmonary emphysema. Investigative radiology. 2004;39(11):681-8. Epub 2004/10/16. PubMed PMID: 15486529.

18. Shamonin DP, Bron EE, Lelieveldt BP, Smits M, Klein S, Staring M, Alzheimer's Disease Neuroimaging I. Fast parallel image registration on CPU and GPU for diagnostic classification of Alzheimer's disease. Front Neuroinform. 2013;7:50. Epub 2014/01/30. doi: 10.3389/fninf.2013.00050. PubMed PMID: 24474917; PMCID: PMC3893567.

19. Klein S, Staring M, Murphy K, Viergever MA, Pluim JP. elastix: a toolbox for intensity-based medical image registration. IEEE Trans Med Imaging. 2010;29(1):196-205. Epub 2009/11/20. doi: 10.1109/TMI.2009.2035616. PubMed PMID: 19923044.

20. Shah RJ, Diamond JM. Update in Chronic Lung Allograft Dysfunction. Clin Chest Med. 2017;38(4):677-92. Epub 2017/11/13. doi: 10.1016/j.ccm.2017.07.009. PubMed PMID: 29128018.

21. Vasilescu DM, Martinez FJ, Marchetti N, Galban CJ, Hatt C, Meldrum CA, Dass C, Tanabe N, Reddy RM, Lagstein A, Ross BD, Labaki WW, Murray S, Xia M, Curtis JL, Hackett TL, Kazerooni EA, Criner GJ, Hogg JC, Han MK. Non-Invasive Imaging Biomarker Identifies Small Airway Damage in Severe COPD. Am J Respir Crit Care Med. 2019. Epub 2019/02/23. doi: 10.1164/rccm.201811-2083OC. PubMed PMID: 30794432.

22. Martinez CH, Diaz AA, Meldrum C, Curtis JL, Cooper CB, Pirozzi C, Kanner RE, Paine R, 3rd, Woodruff PG, Bleecker ER, Hansel NN, Barr RG, Marchetti N, Criner GJ, Kazerooni EA, Hoffman EA, Ross BD, Galban CJ, Cigolle CT, Martinez FJ, Han MK, Investigators S. Age and Small Airway Imaging Abnormalities in Subjects with and without Airflow Obstruction in SPIROMICS. Am J Respir Crit Care Med. 2017;195(4):464-72. Epub 2016/08/27. doi: 10.1164/rccm.201604-0871OC. PubMed PMID: 27564413; PMCID: PMC5378423.

23. Labaki WW, Gu T, Murray S, Hatt CR, Galban CJ, Ross BD, Martinez CH, Curtis JL, Hoffman EA, Pompe E, Lynch DA, Kazerooni EA, Martinez FJ, Han MK. Voxel-Wise Longitudinal Parametric Response Mapping Analysis of Chest Computed Tomography in Smokers. Acad Radiol. 2019;26(2):217-23. Epub 2018/07/30. doi: 10.1016/j.acra.2018.05.024. PubMed PMID: 30055897; PMCID: PMC6340741.

24. Han MK, Tayob N, Murray S, Woodruff PG, Curtis JL, Kim V, Criner G, Galban CJ, Ross BD, Hoffman EA, Lynch DA, Kazerooni E, Martinez FJ, Copdgene, Investigators S. Association between Emphysema and Chronic Obstructive Pulmonary Disease Outcomes in the COPDGene and SPIROMICS Cohorts: A Post Hoc Analysis of Two Clinical Trials. Am J Respir Crit Care Med. 2018;198(2):265-7. Epub 2018/02/28. doi: 10.1164/rccm.201801-0051LE. PubMed PMID: 29485901; PMCID: PMC6058986.

25. Boes JL, Hoff BA, Bule M, Johnson TD, Rehemtulla A, Chamberlain R, Hoffman EA, Kazerooni EA, Martinez FJ, Han MK, Ross BD, Galban CJ. Parametric response mapping monitors temporal changes on lung CT scans in the subpopulations and intermediate outcome measures in COPD Study (SPIROMICS). Acad Radiol. 2015;22(2):186-94. doi: 10.1016/j.acra.2014.08.015. PubMed PMID: 25442794; PMCID: PMC4289437.

26. Bhatt SP, Soler X, Wang X, Murray S, Anzueto AR, Beaty TH, Boriek AM, Casaburi R, Criner GJ, Diaz AA, Dransfield MT, Curran-Everett D, Galban CJ, Hoffman EA, Hogg JC, Kazerooni EA, Kim V, Kinney GL, Lagstein A, Lynch DA, Make BJ, Martinez FJ, Ramsdell JW, Reddy R, Ross BD, Rossiter HB, Steiner RM, Strand MJ, van Beek EJ, Wan ES, Washko GR, Wells JM, Wendt CH, Wise RA, Silverman EK, Crapo JD, Bowler RP, Han MK, Investigators CO. Association between Functional Small Airway Disease and FEV1 Decline in Chronic Obstructive Pulmonary Disease. Am J Respir Crit Care Med. 2016;194(2):178-84. Epub 2016/01/26. doi: 10.1164/rccm.201511-2219OC. PubMed PMID: 26808615; PMCID: PMC5003216.

27. Regan EA, Hokanson JE, Murphy JR, Make B, Lynch DA, Beaty TH, Curran-Everett D, Silverman EK, Crapo JD. Genetic epidemiology of COPD (COPDGene) study design. COPD.

2010;7(1):32-43. Epub 2010/03/11. doi: 10.3109/15412550903499522. PubMed PMID: 20214461; PMCID: PMC2924193.

28. Sieren JP, Newell JD, Jr., Barr RG, Bleecker ER, Burnette N, Carretta EE, Couper D, Goldin J, Guo J, Han MK, Hansel NN, Kanner RE, Kazerooni EA, Martinez FJ, Rennard S, Woodruff PG, Hoffman EA, Group SR. SPIROMICS Protocol for Multicenter Quantitative Computed Tomography to Phenotype the Lungs. Am J Respir Crit Care Med. 2016;194(7):794-806. Epub 2016/08/03. doi: 10.1164/rccm.201506-1208PP. PubMed PMID: 27482984; PMCID: PMC5074650.

29. Boes JL, Bule M, Hoff BA, Chamberlain R, Lynch DA, Stojanovska J, Martinez FJ, Han MK, Kazerooni EA, Ross BD, Galban CJ. The Impact of Sources of Variability on Parametric Response Mapping of Lung CT Scans. Tomography. 2015;1(1):69-77. Epub 2015/11/17. doi: 10.18383/j.tom.2015.00148. PubMed PMID: 26568983; PMCID: PMC4643661.

SUPPORTING INFORMATION

Additional supporting information may be found online in the Supporting Information section at the end of the article.

TABLES

Table 1: Subject Characteristics at Each Site

	KI	FH	UM
Number of Cases (N)	12	48	12
Age (yrs)	44.7 (15.9)	56.2 (15)	59.3 (12)
Gender (m/f)	7/5	29/19	8/4
Height (cm)	67 (12.8)	74.8 (20.8)	70.9 (16.9)
Weight (kg)	169.7 (8)	169.6 (10.9)	172.5 (5.6)
Diagnosed Post-Tx (years)	1.96 (2.32)	3.04 (2.17)	1.33 (0.71)†
FEV1 (% predicted)	49.5 (21.8)	54.0 (25.8)	61.0 (22.5)
FVC (% predicted)	65.5 (23.0)	81.5 (23.5)*	76.0 (30.3)
FEV1/FVC	0.72 (0.29)	0.55 (0.25)*	0.55 (0.16; N=10)$^{P=0.06}$
TLC (% predicted)	84.0 (31.3)	96.0 (20.0)	112.0 (33.0; N=5)

Note: Data presented as the mean (standard deviation), except for FEV1, FVC, FEV1/FVC and TLC presented as median (interquartile range; number of cases is adjusted). Pairwise differences are indicated as * for Site KI and FH, ** for Site KI and UM, † for Site FH and UM. Continuous variables were tested using a univariable ANOVA controlling for multiple comparisons using the Bonferonni posthoc test. Gender was tested using a Pearson $\chi 2$ test.

Table 2: Correlations of PRM and PET for Each Site

PRM Class	PFT	KI (N=12)	FH (N=48)	UM (N=12)
PRM^{fSAD}	FEV1 (% predicted)	-0.309, 0.329	-0.208, 0.156	**-0.718, 0.002**
	FVC (% predicted)	**0.634, 0.027**	**0.438, 0.002**	-0.473, 0.121
	FEV1/FVC	**-0.778, 0.003**	**-0.682, <0.0001**	**-0.705, 0.023 (N=10)**
	TLC (% predicted)	**0.780, 0.003**	**0.682, <0.0001 (N=47)**	0.154, 0.805 (N=5)
PRM^{PD}	FEV1 (% predicted)	0.530, 0.076	-0.127, 0.391	-0.387, 0.214
	FVC (% predicted)	**-0.725, 0.008**	**-0.516, <0.0001**	-0.194, 0.546
	FEV1/FVC	**0.953, <0.0001**	**0.301, 0.038**	0.255, 0.476 (N=10)
	TLC (% predicted)	**-0.885, <0.0001**	**-0.475, 0.001 (N=47)**	-0.564, 0.322 (N=5)

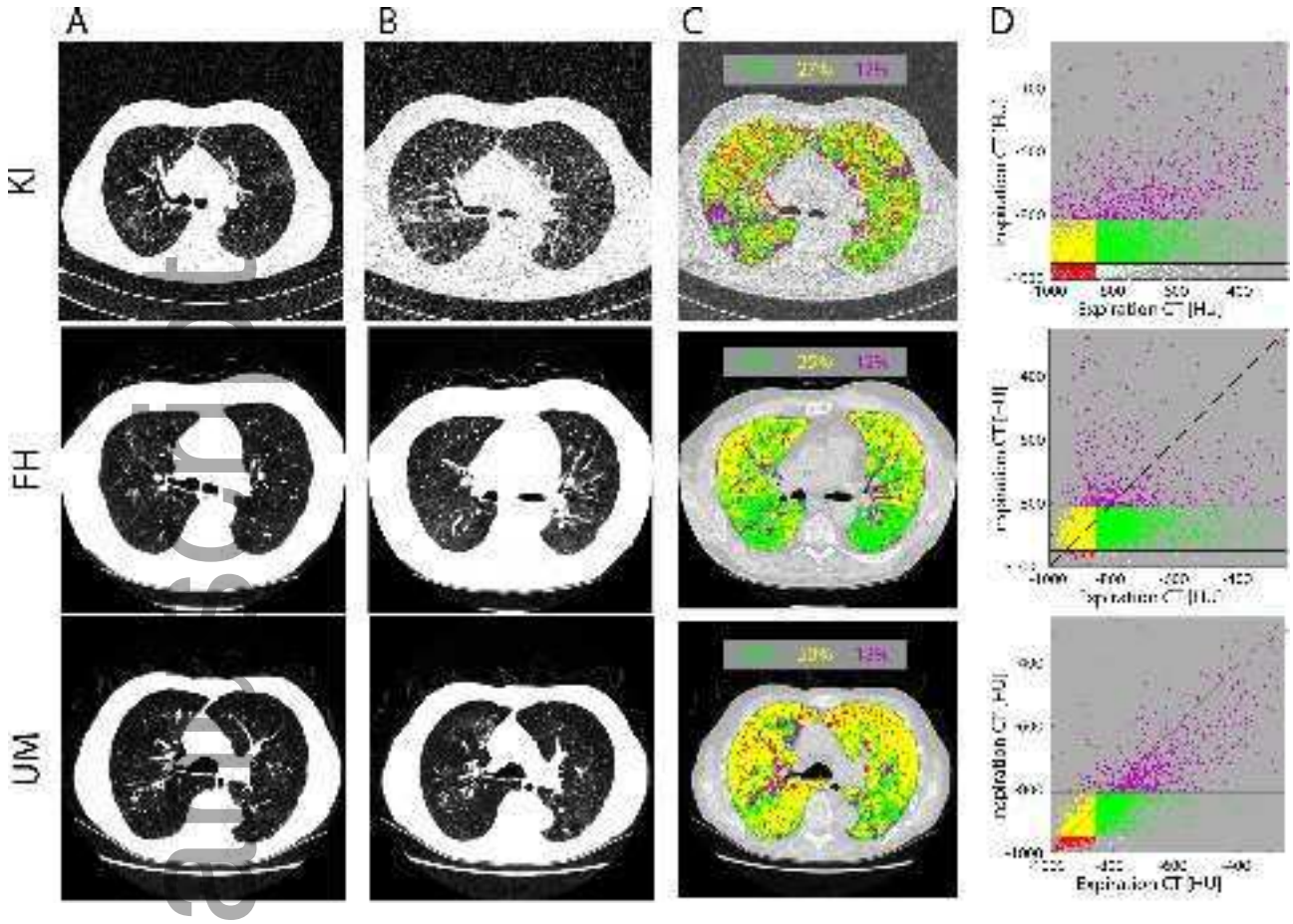

ajt_15814_f1.tif

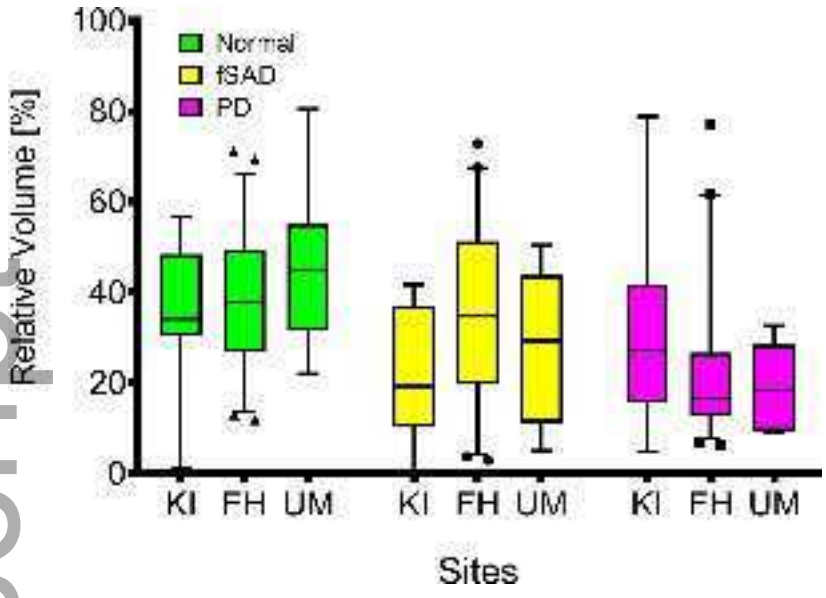

ajt_15814_f2.tif

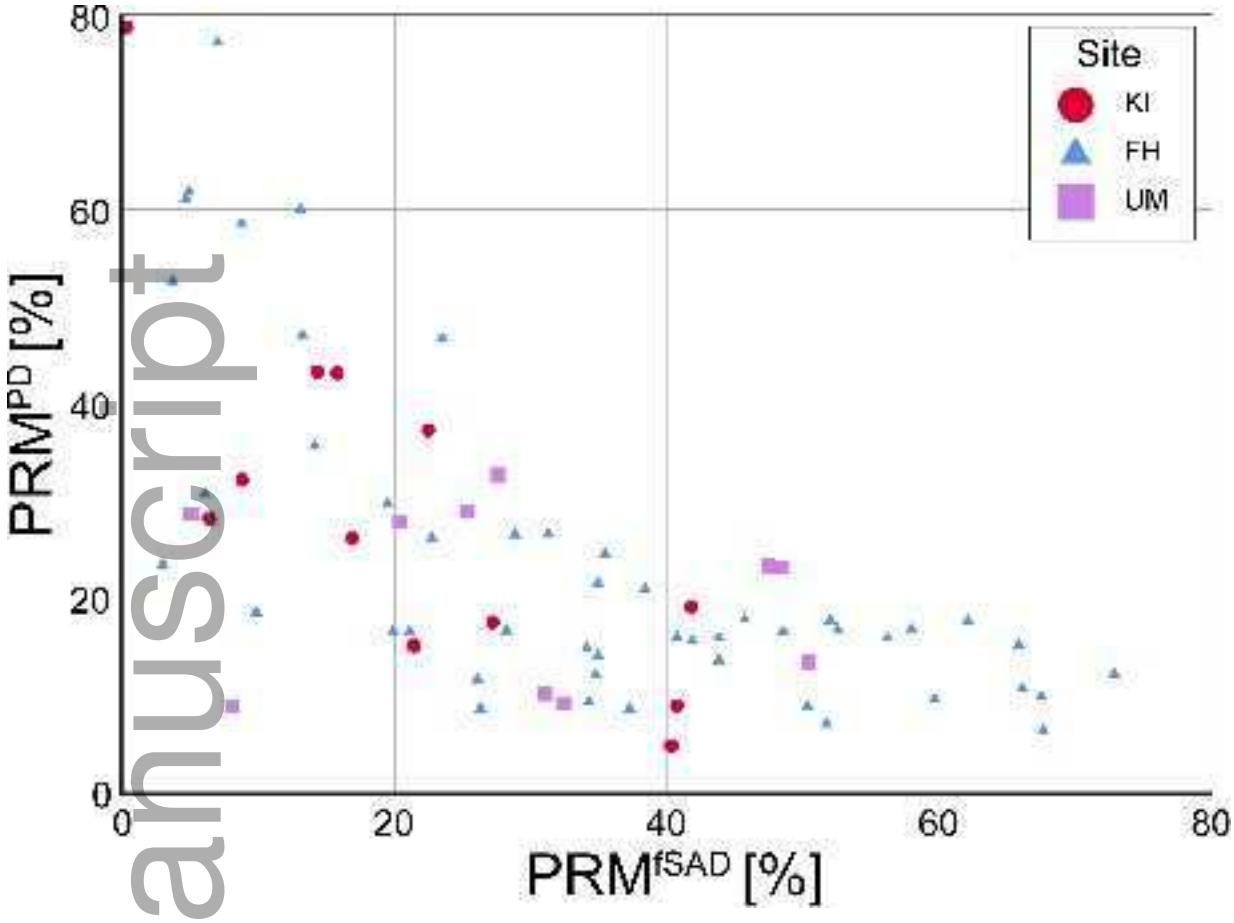

ajt_15814_f3.tif